Systematic parameter study of hadron spectra and elliptic flow from viscous hydrodynamic simulations of Au + Au collisions at $\sqrt{s_{NN}} = 200$ GeV

Chun Shen* and Ulrich Heinz†
Department of Physics, The Ohio State University, Columbus, Ohio 43210-1117, USA

Pasi Huovinen‡
Institut für Theoretische Physik, Johann Wolfgang Goethe-Universität, Max-von-Laue-Straße 1, D-60438 Frankfurt am Main, Germany

Huichao Song§
Department of Physics, The Ohio State University, Columbus, Ohio 43210-1117, USA and
Lawrence Berkeley National Laboratory, 1 Cyclotron Road, MS70R0319, Berkeley, California 94720, USA
(Received 9 October 2010; published 12 November 2010)

Using the $(2+1)$-dimensional viscous hydrodynamic code VISH2 + 1 [H. Song and U. Heinz, Phys. Lett. B **658**, 279 (2008); H. Song and U. Heinz, Phys. Rev. C **77**, 064901 (2008); H. Song, Ph. D. thesis, The Ohio State University, 2009], we present systematic studies of the dependence of pion and proton transverse-momentum spectra and their elliptic flow in 200A GeV Au + Au collisions on the parameters of the hydrodynamic model (thermalization time, initial entropy density distribution, decoupling temperature, equation of state, and specific shear viscosity η/s). We identify a tension between the slope of the proton spectra, which (within hydrodynamic simulations that assume a constant shear viscosity to entropy density ratio) prefer larger η/s values, and the slope of the p_T dependence of charged hadron elliptic flow, which prefers smaller values of η/s. Changing other model parameters does not appear to permit dissolution of this tension.

DOI: 10.1103/PhysRevC.82.054904 PACS number(s): 25.75.Dw, 25.75.Ld, 24.10.Nz, 47.75.+f

I. INTRODUCTION

After experiments at the Relativistic Heavy Ion Collider (RHIC) [1–4] and their theoretical analysis [5–7] established that the quark-gluon plasma (QGP) created in ultrarelativistic heavy-ion collisions is strongly coupled and behaves like an almost ideal fluid ("perfect liquid") with very small viscosity, interest in the theoretical and phenomenological determination of the QGP transport parameters, in particular its specific shear viscosity η/s (i.e., the ratio between its shear viscosity η and entropy density s), soared (see Refs. [8,9] for recent reviews). In principle, it should be possible to extract this quantity from heavy-ion collision experiments by comparing the measured hadron spectra and their azimuthal anisotropies (in particular their elliptic flow) with theoretical simulations of the collision dynamics which treat the QGP shear viscosity as an adjustable parameter [10,11]. In practice, this is a complex and difficult task that requires careful and highly constrained simulations of all dynamical stages of the collision that sandwich the viscous hydrodynamic expansion of the QGP between nonequilibrium phases describing (i) the initial geometry and early evolution of the fireball before its thermalization and (ii) the final kinetic hadron rescattering stage after its hadronization [12,13].

The present work is a contribution to help prepare the path for such a phenomenological extraction of $(\eta/s)_{\rm QGP}$. It employs viscous hydrodynamics to describe the fireball evolution, side-stepping the issues related to early and late nonequilibrium evolution by replacing the output from the (hypothetical) early nonequilibrium evolution model by initial conditions for the hydrodynamic stage (to be adjusted *post facto* to final hadron spectra and multiplicities in central collisions [6]), and the late-stage hadronic rescattering and kinetic freeze-out by a sudden transition from viscous fluid to free-streaming particles, using the Cooper-Frye algorithm [14] along a hypersurface of constant temperature $T_{\rm dec}$. This generalizes analogous attempts to describe experimental data from 200A GeV Au + Au collisions at RHIC with ideal fluid dynamics [6,15–21] to the case of viscous fluid dynamics. Related work has already been reported in Refs. [10,22]; what distinguishes the present study from these earlier articles is that we use a state-of-the-art equation of state that matches the latest lattice QCD data [23,24] at high temperatures to a realistic, chemically nonequilibrated hadron resonance gas at low temperatures. The construction of this equation of state (EOS) is described in Ref. [25], except that we here implement chemical freeze-out of the stable hadron yield ratios at $T_{\rm chem} = 165$ MeV by imposing appropriate temperature dependent nonequilibrium chemical potentials for each hadron species below $T_{\rm chem}$ [15,16,19,26,27]. This ensures that the final hadron yield ratios from our simulations are consistent with their measured values which indicate chemical equilibrium at temperature $T_{\rm chem} \approx 160$–170 MeV [3,28,29].

The purpose of this study is *not* a detailed viscous hydrodynamic fit to the RHIC data; its goal is rather to build intuition for systematic trends and parameter dependences that will be useful in forthcoming more ambitious fit attempts. One feature that disqualifies the present model study from being taken too seriously in comparison with the experimental data

*Corresponding author: shen@mps.ohio-state.edu
†heinz@mps.ohio-state.edu
‡huovinen@th.physik.uni-frankfurt.de
§HSong@LBL.gov

is our assumption of a constant (i.e., temperature independent) specific entropy η/s. While η/s is probably small in the QGP phase [10,11,30], possibly close to the Kovtun-Starinets-Son (KSS) bound $(\frac{\eta}{s})_{\rm KSS} = \frac{1}{4\pi}$ [31,32], it is expected to increase dramatically in the late dilute hadronic phase [33,34]. This can have important consequences for the evolution of flow in relativistic heavy-ion collisions [35] which will be studied in a separate article [36].

II. HYDRODYNAMIC EQUATIONS, INITIAL AND FINAL CONDITIONS

In this work, we use viscous hydrodynamics to simulate the collision system by solving the second-order Israel-Stewart equations as described in Ref. [37]. The energy-momentum tensor of the fluid is decomposed as

$$T^{\mu\nu} = eu^\mu u^\nu - (p + \Pi)\Delta^{\mu\nu} + \pi^{\mu\nu}, \tag{1}$$

where e is the local energy density, p is the thermal equilibrium pressure [given by the equation of state $p(e)$, see below], u^μ is the local flow four-velocity, $\Delta^{\mu\nu} = g^{\mu\nu} - u^\mu u^\nu$ is the spatial projector in the local fluid rest frame, Π is the bulk viscous pressure (which we set to zero in this article, assuming that effects from bulk viscosity can be ignored relative to those caused by shear viscosity [38]), and $\pi^{\mu\nu}$ is the traceless and symmetric shear pressure tensor satisfying $u_\mu \pi^{\mu\nu} = 0$. The equations of motion are the hydrodynamic equations

$$d_\mu T^{\mu\nu} = 0, \tag{2}$$

where d_μ denotes the covariant derivative in curvilinear (τ, x, y, η) coordinates (see Refs. [37,39] for details), coupled to the Israel-Stewart [37,40–42] evolution equations for the viscous pressure components:

$$\Delta^{\mu\alpha}\Delta^{\nu\beta}\dot{\pi}_{\alpha\beta} = -\frac{\pi^{\mu\nu} - 2\eta\sigma^{\mu\nu}}{\tau_\pi} - \frac{\pi^{\mu\nu}}{2}\frac{\eta T}{\tau_\pi} d_\lambda\left(\frac{\tau_\pi}{\eta T}u^\lambda\right). \tag{3}$$

The dot on the left-hand side stands for the local comoving time derivative $D = u^\mu d_\mu$, η is the shear viscosity, $\sigma^{\mu\nu} = \nabla^{\langle\mu} u^{\nu\rangle}$ is the velocity shear tensor (see Refs. [37,39] for notation), and τ_π is the microscopic relaxation time that controls the evolution of $\pi^{\mu\nu}$ (we take $\tau_\pi = 3\frac{\eta}{sT}$ [37]).

The equations are solved numerically in the two transverse spatial directions and time, using the $(2+1)$-dimensional hydrodynamic code VISH2+1 [13,43,44], assuming boost-invariant longitudinal expansion along the beam direction. The net baryon density and heat conductivity are set to zero.

To initialize the hydrodynamic evolution we must specify the starting time τ_0 at which the system is sufficiently close to local thermal equilibrium for viscous hydrodynamics to be applicable, initial energy density and velocity profiles, and the initial viscous pressure tensor $\pi^{\mu\nu}$. We here consider τ_0 as a tunable parameter and vary it between 0.2 and 0.8 fm/c in order to study how it affects the final hadron spectra and elliptic flow.

For the initial energy density profile we study both Glauber [44–47] and color glass condensate (CGC-fKLN) initializations [48–51] in the optical limit (i.e., without accounting for event-by-event fluctuations [52–57]). Figure 1 shows a comparison of typical initial energy density profiles generated

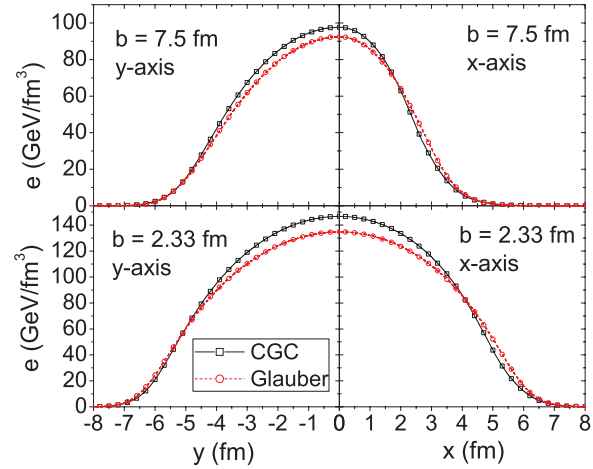

FIG. 1. (Color online) A comparison of initial energy density profiles at $\tau_0 = 0.4$ fm/c for "central" ($b = 2.33$ fm, bottom) and "peripheral" ($b = 7.5$ fm, top) Au + Au collisions from the Glauber and CGC-fKLN models. Shown are cuts along the x axis (right panels) and y axis (left panels). The two profiles are normalized to the same total entropy at $b = 2.33$ fm, using the EOS s95p-PCE to convert energy to entropy density.

from Glauber and CGC initializations. In the Glauber model we assume a mixture of 85% wounded nucleon and 15% binary collision contributions to the entropy production [58]. For the CGC model we assume that the energy density is proportional to the produced gluon energy density distribution, computed with the publicly available fKLN code [59]. In central Au + Au collisions, both profiles are normalized to the same total entropy (adjusted to reproduce the total final charged hadron multiplicity $dN_{\rm ch}/dy$ in these collisions) and converted to energy density using the equation of state s95p-PCE (see next section). With this normalization, both initializations correctly describe the centrality dependence of $dN_{\rm ch}/dy$ for *ideal* fluid dynamics (i.e., for isentropic expansion).

In the viscous case, viscous heating produces additional entropy, resulting in larger final multiplicities which we must correct for by renormalizing the initial entropy density profile in such a way that the final multiplicity is held fixed. We perform this renormalization for the 5% most central Au + Au collisions (i.e., at $b = 2.33$ fm) and then keep the resulting normalization constant fixed for noncentral collisions, i.e., we again assume that the models produce the correct dependence of initial entropy production on collision geometry. It is known, however, that the fractional increase of the final entropy over its initial value due to viscous heating depends on the size of the collision fireball [37] and is therefore expected to be larger in peripheral than central Au + Au collisions. For the results presented in this article, we have checked that the centrality dependence of viscous entropy production is sufficiently weak so that it does not strongly modify the centrality dependence of $dN_{\rm ch}/dy$.

Figure 1 shows that the energy density profile from the CGC initialization has a steeper surface gradient than the Glauber profile. This leads to larger radial acceleration (i.e., radial flow develops more quickly) and is also in part responsible for the larger spatial eccentricity of the CGC profiles at

nonzero impact parameters when compared to the Glauber eccentricities [58,60].

The shear viscous pressure tensor $\pi^{\mu\nu}$ is initialized with its Navier-Stokes value $\pi^{\mu\nu} = 2\eta\sigma_0^{\mu\nu}$, where $\sigma_0^{\mu\nu}$ is the velocity shear tensor at time τ_0, calculated from the initial Bjorken velocity profile, $u^\mu = (u^\tau, u^x, u^y, u^\eta) = (1, 0, 0, 0)$.

For the medium's viscous properties the shear viscosity η/s is the key parameter. According to perturbative and lattice QCD, the temperature dependence of η/s is weak over the range explored in heavy-ion collisions at RHIC energies. This suggests use of a constant ratio η/s. In this work, the value of η/s is tuned from 0.08 to 0.24 in order to study the effects of shear viscosity on the hadron spectra and elliptic flow. The influence of a temperature-dependent η/s will be explored in a forthcoming article [36].

Final-state hadron spectra are calculated from the hydrodynamics output via the Cooper-Frye procedure [14]

$$E\frac{d^3N_i}{d^3p} = \frac{g_i}{(2\pi)^3}\int_\Sigma p\cdot d^3\sigma(x) f_i(x,p), \tag{4}$$

where Σ is the freeze-out surface with normal vector $d^3\sigma_\mu(x)$. We take for Σ an isothermal surface; calculations for different freeze-out temperatures are presented in Sec. IV B. After computing the spectra of all hadronic resonances included in EOS s95p-PCE from Eq. (4), we use the resonance decay program [61,62] from the AZHYDRO package[1] to let the unstable resonances decay. The pion and proton spectra shown in this work include all decay products from strong decays.

The distribution function on the freeze-out surface can be decomposed as $f = f_{\rm eq} + \delta f$ into a local equilibrium part

$$f_{\rm eq}(p,x) = \frac{1}{e^{p\cdot u(x)/T(x)} \pm 1} \tag{5}$$

and a (small) deviation δf from local equilibrium due to shear viscous effects for which we make the quadratic ansatz [63,64] (for other possibilities see Ref. [65]) using

$$\delta f(x,p) = f_{\rm eq}(p,x)[1\mp f_{\rm eq}(p,x)]\frac{p^\mu p^\nu \pi_{\mu\nu}(x)}{2T^2(x)[e(x)+p(x)]} \tag{6}$$

[the upper (lower) sign is for fermions (bosons)] for all particle species. δf is proportional to the shear viscous pressure tensor $\pi^{\mu\nu}(x)$ on the freeze-out surface and increases (in our case) quadratically with the particle momentum.

III. EQUATION OF STATE

To solve Eqs. (2) and (3) one has to know the equation of state $p(e)$ (EOS) of the medium. In this work we compare three different equations of state to study how the EOS affects the hadron spectra and elliptic flow. Two of them, SM-EOS Q [44] and EOS L [37], are well known in the literature; the former implements a (slightly smoothed) first-order phase transition between an ideal massless parton gas and a hadron resonance gas (HRG), and the second is a rough attempt to match lattice QCD (LQCD) data [66] above T_c to the HRG in a smooth crossover transition, as seen in LQCD (see also Ref. [67]). In both cases, the system is assumed to be in chemical equilibrium all the way down to kinetic freeze-out at temperature $T_{\rm dec}$.

Our third equation of state, s95p-PCE, also interpolates between the HRG at low temperature and the lattice EOS at high temperatures, but the matching procedure is more sophisticated than the one used to construct EOS L, and the lattice EOS is based on the recent results by the hotQCD collaboration [23,24]. Furthermore, below $T_{\rm chem} = 165$ MeV, the EOS is that of a *chemically frozen* HRG. The matching procedure using a chemically equilibrated HRG is explained in detail in Ref. [25]. The procedure for the chemically frozen HRG is identical since the chemical freeze-out temperature is below the temperature where the interpolated EOS deviates from the HRG EOS.

However, the version of s95p-PCE used here deviates slightly from the s95p-PCE-v1 EOS shown in Appendix C of Ref. [25]. First, we have chosen $T_{\rm chem} = 165$ MeV for the chemical freeze-out temperature, as fitted to experimental data using thermal models [3,28,29], and we have considered as stable particles those with a half-life larger than 40 fm/c instead of 10 fm/c. Second, our s95p-PCE corresponds to a historically slightly earlier stage of the parametrization of the EOS than the final version published in Ref. [25]: The fit to the lattice data was done without the $T = 630$ MeV data point. This causes at most 0.4% difference between this version and the final version of the EOS. We have checked that such a small difference does not cause observable consequences in the fluid-dynamical evolution.[2]

We have built the EOS of the chemically frozen hadron gas using the standard procedure in the literature: Below $T_{\rm chem}$ the ratios of stable hadron yields are fixed to their chemical equilibrium values at $T_{\rm chem}$ by finite nonequilibrium chemical potentials $\mu_i(T)$ [15,16,19,26,27]. It is worth noting that the ratios of individual particle densities are not conserved. What is conserved are the ratios of the *total densities* of stable particles, $\bar{n}_i$, where total density means the sum of the actual density of species i and the additional density of the same species that would arise if all unstable resonances in the system were allowed to immediately and irreversibly decay. The rapid processes that form and decay resonances through strong interactions are still in equilibrium, and thus the resonance populations are in equilibrium with the populations of their daughter particles (see Refs. [15,26] for a detailed discussion). Thus the chemically frozen system is in a state of partial chemical equilibrium (PCE).

In practice the chemically frozen EOS is evaluated assuming that the evolution is isentropic and the ratios $\bar{n}_i/s$ stay constant. Strictly speaking this is not the case in viscous hydrodynamics since dissipation causes an increase in entropy. However, we have checked that in our calculations the viscous entropy production from fluid cells with temperatures below $T_{\rm chem} = 165$ MeV is small (see also the right panel of

[1] AZHYDRO is available at the URL [http://www.physics.ohio-state.edu/~froderma/].

[2] For a discussion of the uncertainties in parametrizing the lattice data and its effect on fluid dynamics see Ref. [25].

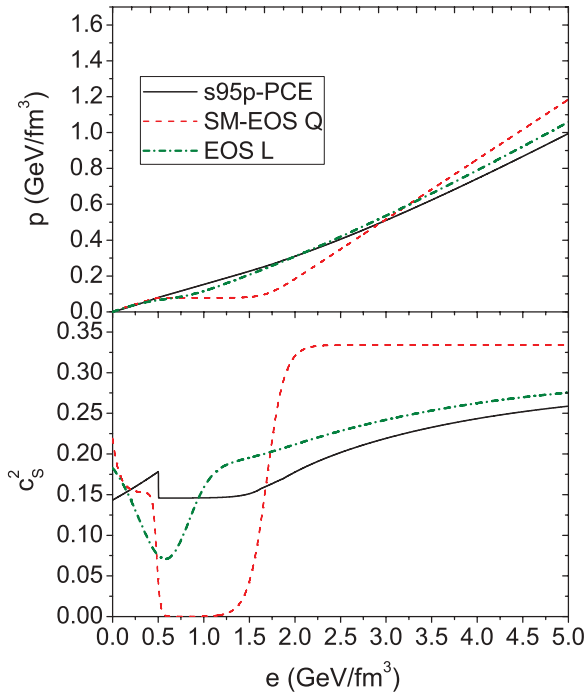

FIG. 2. (Color online) The three equations of state, s95p-PCE, SM-EOS Q, and EOS L, used in this article. The lower panel shows the squared speed of sound $c_s^2 = \frac{\partial p}{\partial e}$ as a function of energy density e, whereas $p(e)$ is shown in the upper panel.

Fig. 8 in Ref. [37]) and our EOS is a good approximation of the physical EOS.

An analytic parametrization of s95p-PCE is given in Appendix; the EOS can be obtained in a tabulated form at Ref. [68], where the particles included in the hadron resonance gas are also listed. (We included all resonances listed in the summary of the 2004 edition of the *Review of Particle Physics* [69] up to 2 GeV mass. Note that our s95p-PCE is called s95p-PCE165-v0 at Ref. [68] to differentiate it from other versions of the parametrization.)

The three equations of state are compared in Fig. 2. The upper panel shows the pressure and the lower panel the squared speed of sound as a function of e. The spike in $c_s^2(e)$ at $e \sim 0.5$ GeV/fm^3 results from the sudden breaking of chemical equilibrium at $T_{\rm chem} = 165$ MeV. It has negligible consequences for the expansion dynamics. Figure 2 shows that s95p-PCE is a much softer EOS than SM-EOS Q in the QGP phase above T_c but much harder in the phase transition region around T_c. Contrary to SM-EOS Q and EOS L, the rapid crossover transition between quarks and hadrons that is realized by nature does not have a well-defined "softest point" [70] which would cause the fireball to spend an extended time period in the critical region. Instead, the speed of sound never drops much below its value in the HRG, causing the fireball to cool rapidly through the phase transition [71].

IV. SPECTRA AND ELLIPTIC FLOW

In this section, we discuss the dependence of the transverse-momentum spectra in central 200A GeV Au + Au collisions (0–5% centrality, $b = 2.33$ fm) and the elliptic flow $v_2(p_T)$ in semiperipheral collisions (20–30% centrality, $b = 7.5$ fm) for pions, protons, and (for v_2) all charged hadrons on the EOS and various input parameters discussed in Secs. II and III. We have also checked that everything we say below about the central collision spectra also applies, at the same level of precision, to the ϕ-averaged spectra in semiperipheral collisions.

Since the amount of viscous heating depends on the input parameters, for each case we retune the normalization of the initial energy density profile *in central collisions* so the same final π^+ multiplicity density dN_{π^+}/dy is obtained. Its value is adjusted by eye such that an optimal fit to the measured pion spectrum is obtained in the low-p_T region, $p_T < 1.5$ GeV/c. As there are slight discrepancies between the published data from the STAR and PHENIX Collaborations, and these experiments give their results in different centrality bins, we have decided to concentrate on PHENIX results [72–74] when comparing the theoretical curves with experimental data. Since we do not attempt to fit these data but use the comparison only to illustrate trends, this procedure is acceptable. A future serious dynamical model fit to the data will require proper accounting for systematic uncertainties and discrepancies among the different experiments.

Since viscous heating effects are relatively more important in peripheral than in central collisions, our renormalization to constant multiplicities at $b = 2.33$ fm leads to slightly different pion multiplicities at larger impact parameters. For a given EOS, ensuring the same final pion multiplicity is equivalent to ensuring the same final total multiplicity. For different equations of state (see Sec. IV D) identical pion multiplicities correspond to slightly different total multiplicities.

In the following we show hadron spectra and elliptic flow up to transverse momenta of 3 GeV/c. We emphasize that this is for illustrative purposes only and does not imply that we believe hydrodynamics to provide a valid description up to such large p_T. When comparing model results with experimental data, we judge the quality of agreement by focusing on the region $p_T < 1.5$ GeV/c for pions and $p_T < 2.5$ GeV/c for protons (which is where we believe hydrodynamics is a reliable approach [75]). Specifically for pions, if the calculated spectra drop off more steeply than the measured ones above $p_T = 1.5$ GeV/c, we discount this discrepancy, noting that this is the region where the experimental spectra begin to change from an exponential to a power-law shape due to the onset of hard physics.

A. η/s dependence at fixed $\tau_0 = 0.4$ fm/c and $T_{\rm dec} = 140$ MeV

Transverse-momentum spectra of pions and protons in the most central Au + Au collision are shown in Fig. 3 and in the upper left panel of Fig. 4. The spectra include all strong resonance decays. Here we hold initial and final conditions fixed (except for a renormalization of the initial peak energy density to ensure the same final multiplicity in all calculations) and vary the specific shear viscosity η/s (see figure captions for details). One sees that under these conditions larger η/s values result in flatter spectra; the effect is particularly strong for protons at low p_T. The main reason is that larger shear viscosity leads to larger radial flow, due to a positive contribution from

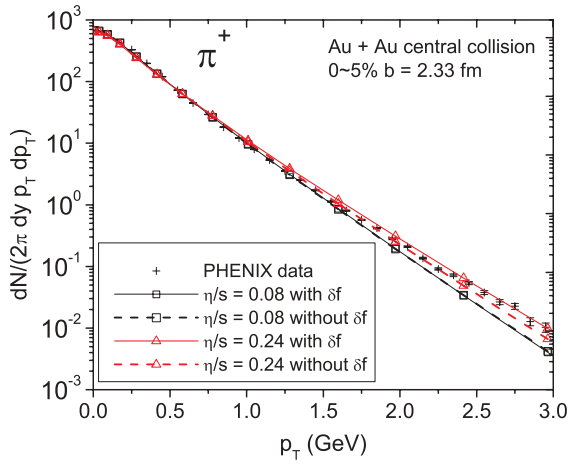

FIG. 3. (Color online) Pion spectra for 200A GeV Au + Au collisions at 0–5% centrality from VISH2+1 compared with PHENIX data [72]. Results for two different constant values of η/s (0.08 and 0.24) are shown; strong resonance decays are included. Solid and dashed lines show the spectra calculated from the full distribution function $f = f_{\rm eq} + \delta f$ ("with δf") and from the equilibrium part only ("without δf"). The hydrodynamic evolution starts at $\tau_0 = 0.4$ fm/c with an initial CGC energy density profile and ends at $T_{\rm dec} = 140$ MeV. The EOS is s95p-PCE.

$\pi^{\mu\nu}$ to the effective transverse pressure gradients at early times [39,76,77].

Figure 3 identifies, however, a second contribution to the viscous hardening of the spectra: For $\eta/s = 0.16$ and 0.24 and evolution with s95p-PCE, we find that the viscous correction due to the nonequilibrium deviation δf of the distribution function on the freeze-out surface, Eq. (6), is *positive* for $p_T \gtrsim 0.5$–1 GeV/c,[3] thus adding to the hardening of the spectra from radial flow.[4] This is the same sign for δf as found in Ref. [78] (for a different EOS) but opposite to what had been found earlier with VISH2+1 for smaller values of η/s using SM-EOS Q (i.e., a first order phase transition) [44]. (For $\eta/s = 0.08$ Fig. 3 shows a *negative* δf correction for pions at large p_T of the *same* sign but much smaller magnitude than found earlier [44] with Glauber initial conditions and SM-EOS Q). Our finding confirms the fragility of the sign of δf that was already discussed in Ref. [44].[5]

We note in passing that the positive δf at large p_T found here with s95p-PCE is found to be largest in near-central collisions ($b \approx 0$) where it can even lead to a *positive* δf correction to the differential elliptic flow $v_2(p_T)$. At larger b, the δf contribution to $v_2(p_T)$ remains negative here (see right panels of Fig. 4), as has been consistently observed in other work [10,43,44,78,79].

The time-integrated effect of the shear viscous pressure on the radial flow and the "instantaneous" effect of the viscous correction δf to the distribution function on the freeze-out surface together give the total shear viscous correction to the hadron spectra. For $\eta/s = 0.08$ we see in Fig. 3 that with s95p-PCE the δf correction to the pion spectrum is almost negligible, but the upper left panel in Fig. 4 shows that the pion and proton spectra are still flatter than for the ideal fluid, reflecting the larger radial flow caused by the shear viscous increase of the transverse pressure gradients [44]. Thus both the effect of viscosity on radial flow *and* δf contribute to the flattening of the hadron spectra.

Comparing with the experimental data we find that both pion and proton spectra favor a relatively large shear viscosity, $\eta/s = 0.16 \sim 0.24$. We caution that this conclusion is based on calculations done with constant (i.e., temperature independent) η/s and may be subject to revision once one properly accounts for the increase of η/s in the dilute late hadronic stage.

Proceeding to the elliptic flow, we start with a discussion of the charged hadron v_2 in the lower left panel of Fig. 4. Here, larger shear viscosity values are seen to lead to a stronger suppression of elliptic flow. The right panels in Fig. 4 show that this suppression is again the consequence of two additive effects: shear viscosity reduces the buildup of anisotropic collective flow, reflected in the equilibrium part $f_{\rm eq}$ of the distribution function on the freeze-out surface (dotted lines in Fig. 4), but the viscous correction δf causes an additional suppression of v_2. For T-independent η/s, both suppression effects increase monotonically with shear viscosity; however, the increase of the δf correction with rising η/s is weaker than that of the viscous suppression of the collective flow anisotropy. The stronger suppression of v_2 for larger η/s is thus mostly due to the viscous suppression of anisotropic flow.

Since elliptic flow data for identified pions and protons in the particular centrality bin shown in Fig. 4 are not yet available, we compare in the lower left panel with experimental data for unidentified charged hadrons. This plot suggests that, even for CGC initial conditions which produce more eccentric fireballs than the Glauber model [10,58], the v_2 data suggest a smaller value for η/s, $\eta/s = 0.08$–0.16, than obtained from the p_T spectra for central collisions.

This tension between the slope of the p_T spectra (which tends to favor larger η/s values) and the p_T dependence of v_2

[3]The Landau matching conditions require the δf correction to integrate to zero when summing over all momenta, so a positive δf contribution at high p_T implies a negative δf contribution at low and/or intermediate p_T. In Ref. [44] we found that it typically changes sign twice.

[4]We checked that for all equations of state studied here that the sign of δf at high p_T does not depend on whether we use CGC or Glauber initial conditions.

[5]For EOS L and SM-EOS Q and $\eta/s > 0.08$, we find a negative sign of the δf contribution to both pion and proton spectra at high p_T, while the corresponding contribution is positive in the case of s95p-PCE. The negative sign appears to be correlated with the use of an EOS with a "softest point." From ideal fluid dynamic simulations with such first-order or almost-first-order phase transitions we know that the rapid change of c_s^2 in the transition region generates strong structures in the radial velocity profile in fireball regions that are close to the critical temperature [46] and that these structures partially survive until the matter has reached decoupling. We suspect that velocity gradients associated with these structures play an important role in generating for EOS L and SM-EOS Q a negative δf contribution to the spectra at high p_T.

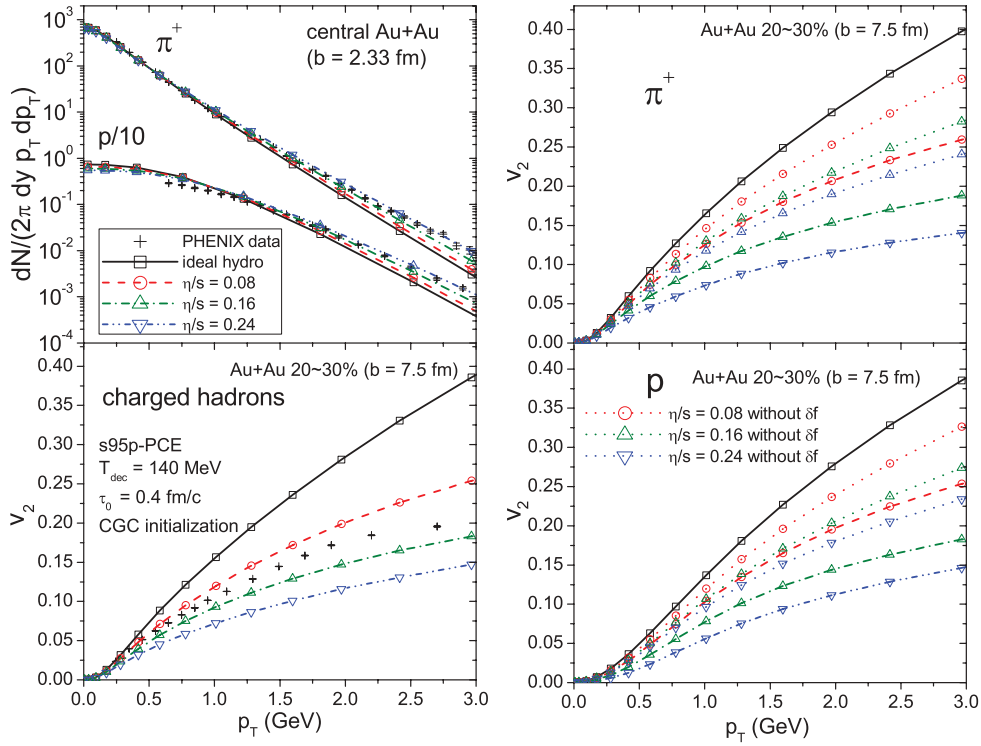

FIG. 4. (Color online) (Upper left panel) Transverse-momentum spectra $dN/(dyd^2p_T)$ for pions and protons from VISH2+1 for the 5% most central Au + Au collisions ($b = 2.33$ fm) compared with experimental data from the PHENIX Collaboration [72]. (Lower left panel) Differential elliptic flow $v_2(p_T)$ for charged hadrons from Au + Au collisions at 20–30% centrality ($b = 7.5$ fm) compared with PHENIX data [73]. (Right panels) $v_2(p_T)$ for pions (top) and protons (bottom). In these panels we compare the elliptic flow computed from the full distribution function $f = f_{\rm eq} + \delta f$ (dashed, dot-dashed, and double-dot-dashed lines) with the contribution from the equilibrium part only (dotted lines, "without δf"). Lines with different symbols show calculations for different constant values of the specific shear viscosity η/s, ranging from 0 (ideal hydro, solid lines) to 0.24 as indicated. All strong resonance decays are included; charged hadrons comprise $\pi^{\pm}$, $K^{\pm}$, p, $\overline{p}$, $\Sigma^{\pm}$, $\overline{\Sigma}^{\mp}$, Ξ^{-}, $\overline{\Xi}^{+}$, Ω^{-}, and $\overline{\Omega}^{+}$. The EOS and initial and final conditions are the same as in Fig. 3.

(which favors smaller values) is generic and, as far as we were able to ascertain, cannot be resolved with purely hydrodynamic calculations that assume constant η/s. A possible solution of this problem will likely involve accounting for temperature dependence of η/s and/or the transition to a microscopic kinetic description for the late hadronic stage.

B. $T_{\rm dec}$ dependence at fixed $\tau_0 = 0.4$ fm/c and $\eta/s = 0.16$

In Fig. 5 we explore the sensitivity of spectra and elliptic flow on the value of the decoupling temperature, holding all other parameters fixed. For the constant η/s we select $\eta/s = 0.16$ as a compromise between the values preferred by the proton spectra and charged hadron v_2, respectively, in Fig. 4.

The left upper panel shows that lower freeze-out temperatures lead to flatter proton spectra. This is a consequence of additional radial flow built up during the extra time the fireball needs to cool down to lower $T_{\rm dec}$. As is well known [80,81], the heavier protons receive a larger push to higher p_T from radial flow than the lighter pions. Indeed, Fig. 4 shows that the pion spectra become *steeper* as $T_{\rm dec}$ is lowered [82]. Since pions are almost massless on the scale of measured transverse momenta, the inverse slope of their p_T spectrum can be approximated by the relativistic blueshift formula [80,81] $T_{\rm slope} = T_{\rm dec}\sqrt{\frac{1+\langle v_\perp\rangle}{1-\langle v_\perp\rangle}}$, where $\langle v_\perp\rangle$ is the average radial flow at $T_{\rm dec}$. For pions, the steepening effects on their spectrum from decreasing $T_{\rm dec}$ overwhelm the flattening effects resulting from the associated increase of $\langle v_\perp\rangle$, causing a net softening of the pion spectra for lower freeze-out temperatures.

From the lower left panel of Fig. 5 one sees that lower decoupling temperatures lead to larger elliptic flow $v_2(p_T)$ for charged hadrons. To fully understand this systematics it is worth comparing charged hadrons to the p_T spectra and $v_2(p_T)$ of pions (upper left and right panels, respectively) which dominate the charged hadron yield. The observed tendency reflects a combination of three effects:

(i) Since the p_T spectrum of pions (which dominate the charged hadrons) gets steeper, even the same hydrodynamic momentum anisotropy would lead to a larger slope of $v_2(p_T)$, to compensate for the lower yield at high p_T.

(ii) Since the fireball has not lost all of its eccentricity by the time the QGP converts to hadrons [44], additional momentum anisotropy is generated during the hadronic stage. Lower decoupling temperatures give the system time to develop more momentum anisotropy, leading to a larger v_2. If the p_T spectrum stays unchanged or gets

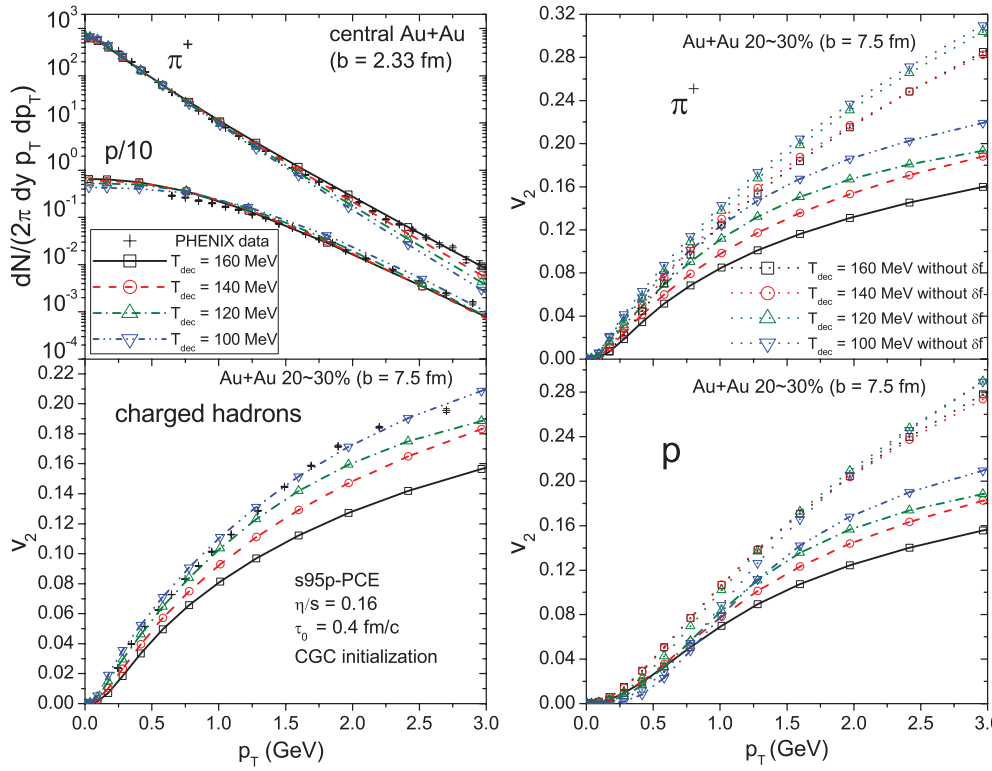

FIG. 5. (Color online) Similar to Fig. 4 but for fixed $\eta/s = 0.16$ and varying decoupling temperature $T_{\rm dec}$ ranging from 100 to 160 MeV as indicated.

steeper (as is the case for pions in Fig. 5), a larger v_2 must lead to a larger $v_2(p_T)$. The combination of effects (i) and (ii) is seen in the dotted lines in the upper right panel, which reflect the hydrodynamic flow anisotropy at decoupling, undistorted by viscous corrections δf to the local equilibrium distributions at freeze-out. The effect (ii) decreases with increasing η/s in the hadronic phase (not shown here), so the combined effect may be weaker than seen in Fig. 5 if viscous hydrodynamics is replaced by a microscopic hadron cascade such as UrQMD in the hadronic phase.

(iii) The (negative) viscous corrections from δf to v_2 are smaller at lower temperatures, due to the general decrease of the viscous pressure components [44]. This contributes the largest fraction of the observed increase of $v_2(p_T)$ with decreasing $T_{\rm dec}$, especially at large p_T.

Combining the information from the two left panels in Fig. 5 we conclude that both the proton spectra in central collisions and charged hadron $v_2(p_T)$ in peripheral collisions favor decoupling temperatures near the lower end of the window studied here (i.e., $T_{\rm dec} = 100$ MeV works better than $T_{\rm dec} = 140$ MeV). The pion spectra are affected by variations of $T_{\rm dec}$ mostly at $p_T \gtrsim 1$–1.5 GeV/c where they fall increasingly below the experimental data as we lower $T_{\rm dec}$. However, this is also the region where the hydrodynamic description of the pion spectra is known to begin to break down [75], due to the gradual transition from soft to hard physics which causes the pion spectrum to change from an exponential to a power-law shape. Focusing therefore on the region $p_T < 1.5(2.5)$ GeV/c for pions (protons), we conclude that a purely hydrodynamic description of the experimental data favors freeze-out temperatures near 100 MeV.

The right panels of Fig. 5 show how $T_{\rm dec}$ affects the elliptic flow of different identified hadrons. Charged hadrons mostly reflect the behavior of the dominating pions whose $v_2(p_T)$ increases with decreasing freeze-out temperature. But protons behave differently: At low $p_T < 1$ GeV, their elliptic flow decreases with decreasing decoupling temperature, while at high p_T it increases with decreasing $T_{\rm dec}$. The latter feature reflects the increasing hydrodynamic momentum anisotropy and decreasing magnitude of the δf correction, just like it is reflected in the pion and charged hadron v_2. The decrease of proton v_2 at low p_T, on the other hand, is a consequence of having larger radial flow at lower $T_{\rm dec}$ which pushes the protons to larger p_T. So rather than thinking of this effect as a decrease of proton v_2 at fixed p_T, we should think of it as shifting the elliptic flow to larger p_T.

C. τ_0 dependence at fixed $\eta/s = 0.16$ and $T_{\rm dec} = 140$ MeV

The upper left panel of Fig. 6 shows that the pion and proton spectra react similarly to a change of the starting time τ_0 of the hydrodynamic evolution: Smaller τ_0 values lead to more high-p_T particles, reflecting more radial flow. Starting hydrodynamics earlier allows it to generate radial flow earlier, and even though this also causes the fireball to cool down to $T_{\rm dec}$ sooner and freeze out earlier, the net effect is still a slight increase of the average radial flow at freeze-out.

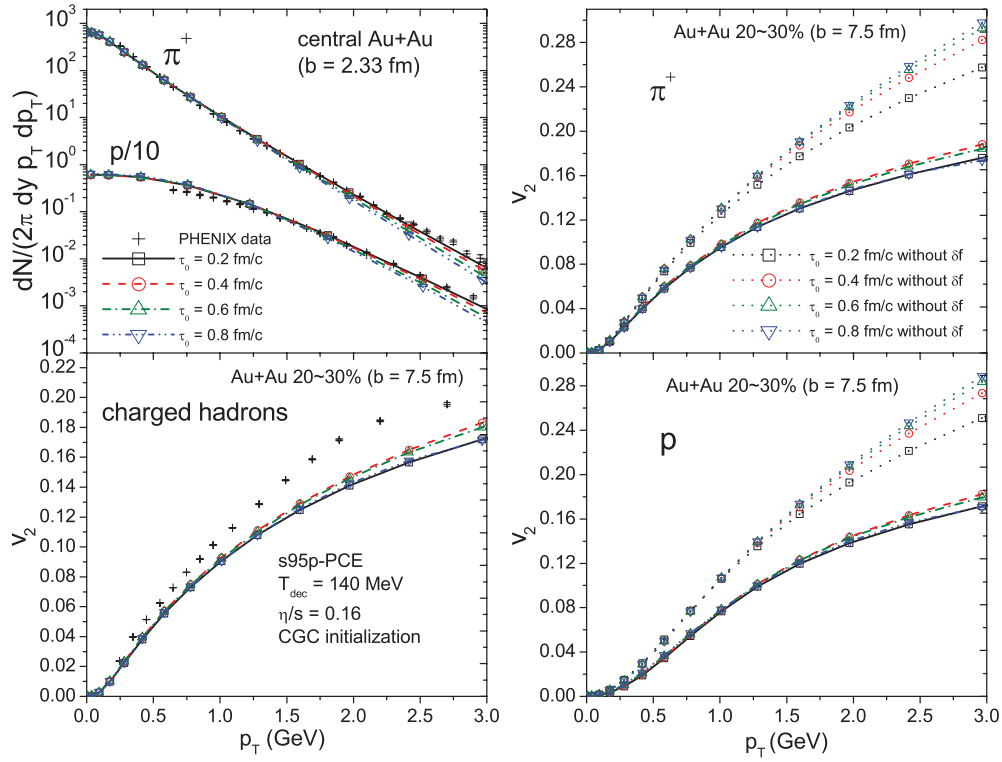

FIG. 6. (Color online) Similar to Fig. 4 but for fixed $\eta/s = 0.16$ and varying starting time τ_0 for the hydrodynamic evolution, ranging from 0.2 to 0.8 fm/c as indicated.

For soft momenta $p_T < 1.5$ GeV/c, the effect of τ_0 on $v_2(p_T)$ is negligible. This is true even for protons, showing that the increase of radial flow with decreasing τ_0 is a small effect and not enough to visibly push the proton v_2 to larger p_T. At higher p_T, the dependence of the charged hadron, pion and proton v_2 on τ_0 is nonmonotonic. The right panels of Fig. 6 show that this nonmonotonic behavior is the result of two counteracting tendencies which both depend on τ_0 monotonically: (i) The elliptic flow computed from the local equilibrium part $f_{\rm eq}$ of the distribution function at freeze-out increases monotonically with increasing τ_0, reflecting the longer total fireball lifetime (and thus the longer time available to build up momentum anisotropy) when the hydrodynamic evolution starts later. (ii) The v_2 suppression resulting from the viscous correction δf at freeze-out also increases monotonically with increasing τ_0. We don't have a complete understanding of why starting (and thus also ending) the hydrodynamics later leads to a larger δf on the decoupling surface; we suspect that since the hydrodynamical flow would eventually settle into a three-dimensional spherically symmetric Hubble flow with no shear stress, starting earlier leads to a stronger transverse flow, and thus to a flow profile which is closer to a spherically symmetric flow at the time of decoupling.

D. EOS dependence at fixed $\tau_0 = 0.4$ fm/c, $\eta/s = 0.16$, and $T_{\rm dec} = 140$ MeV

In Fig. 7 we study the sensitivity of hadron spectra and elliptic flow on the equation of state, holding all other hydrodynamic parameters fixed (except for the normalization of the initial energy density profile which is again adjusted to ensure constant final multiplicity in central Au + Au collisions). We first note that, due to the different chemical composition at hadron freeze-out, the proton yields for EOS L and SM-EOS Q are below those of s95p-PCE if we hold the pion mulitiplicity fixed: In s95p-PCE we prohibit protons from annihilating on antibaryons while such annihilation processes are allowed in the other two equations of state which assume hadrons in chemical equilibrium. To explore flow effects we should concentrate on the *shape* (i.e., inverse slopes) of the pion and proton spectra. We see that EOS L produces the flattest spectra, followed by SM-EOS Q, whereas the spectra from s95p-PCE are steepest. Since all three curves correspond to the same (constant) freeze-out temperature $T_{\rm dec} = 140$ MeV, these differences can only arise from different amounts of radial flow or different δf corrections (i.e., different viscous pressure components $\pi^{\mu\nu}$) along the freeze-out surface. To separate these two effects we plotted the spectra calculated without the δf correction and found the same hierarchy. We conclude that, for fixed freeze-out temperature, s95p-PCE produces the weakest radial flow averaged over the freeze-out surface and EOS L generates the strongest flow, with SM-EOS Q falling in between.

The reasons for s95p-PCE generating less radial flow than the other two equations of state are complex and subtle. The differences in speed of sound during the evolution largely cancel out (see Ref. [25]). The key difference is that, at a fixed freeze-out temperature, the chemically frozen HRG embodied in s95p-PCE has a considerably larger energy density ($e_{\rm dec} = 0.301$ GeV/fm^3 at $T_{\rm dec} = 140$ MeV) than the chemically

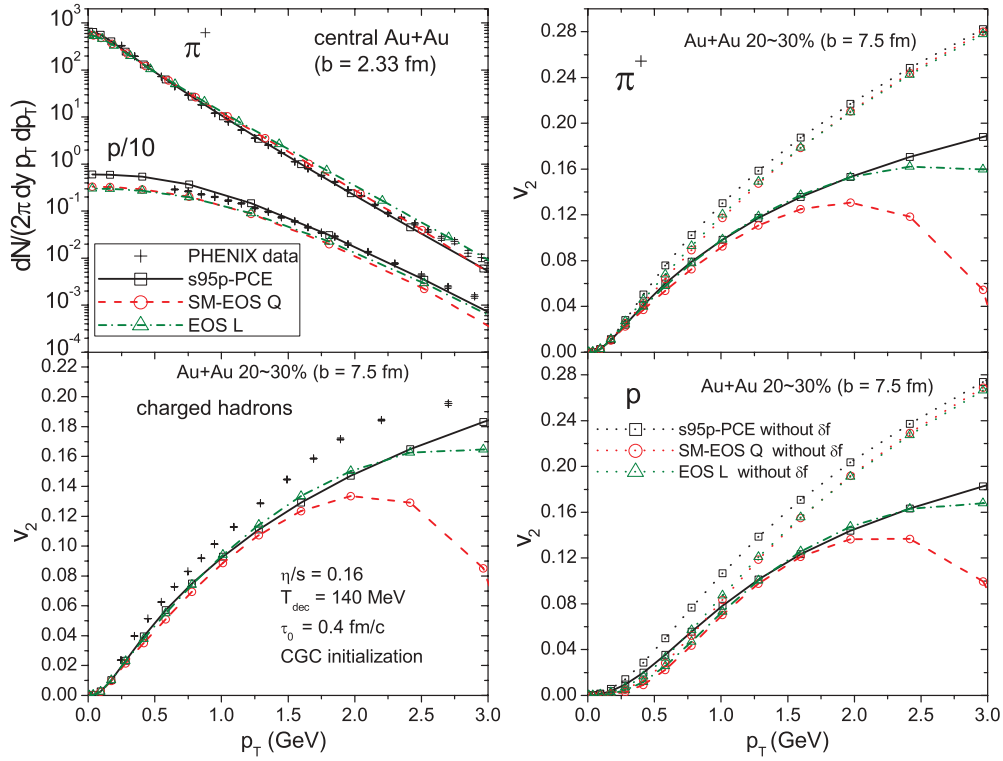

FIG. 7. (Color online) Similar to Fig. 4 but for fixed $\eta/s = 0.16$ and different equations of state (SM-EOS Q, EOS L, and s95p-PCE) as indicated. Since SM-EOS Q and EOS L have different chemical composition than s95p-PCE at $T_{\rm dec} = 140$ MeV, they yield fewer protons than s95p-PCE when normalized to the same pion yield.

equilibrated HRG used in EOS L and SM-EOS Q (which has $e_{\rm dec} = 0.143$ GeV/fm^3 at the same temperature) [15], due to the larger-than-equilibrium abundances of baryon-antibaryon pairs and mesons that are prohibited from annihilating as the system cools below $T_{\rm chem}$. So with s95p-PCE the fireball reaches the freeze-out point earlier, and it has a smaller freeze-out radius. It is this latter feature which causes the average radial flow along the freeze-out surface to be smaller for s95p-PCE than for the other two EOS: when plotting the radial velocity profiles along the decoupling surface, we found that all profiles are approximately linear functions of the radial distance r from the center (qualitatively similar to the profiles shown in Fig. 4 of Ref. [83]) and that the profile for s95p-PCE has the *largest* slope. However, the average radial flow is *smallest* because for s95p-PCE the average over the freeze-out surface is truncated at a smaller maximal r value.

The charged hadron, pion and proton elliptic flows $v_2(p_T)$ show quite large sensitivity to the EOS, especially at high p_T. (We repeat that the hydrodynamic spectra should probably not be trusted beyond $p_T \sim 2$–2.5 GeV/c, but plotting them out to 3 GeV/c makes it easier to see what is going on in the calculation.) But we see that most of this sensitivity comes in through the δf correction at freeze-out which is particularly large for SM-EOS Q. The reason for this is that the first-order phase transition leads to large velocity gradients at the QGP-to-mixed-phase and mixed-phase-to-HRG interfaces [46] which are largely but not completely washed out by viscous effects [44] and leave traces on the decoupling surface. δf effects are weaker with the smoother EOS L than with SM-EOS Q even though EOS L generates on average more radial flow.

To discuss the contribution from collective flow anisotropies to pion and proton $v_2(p_T)$ we focus on the dotted lines in the right panels of Fig. 7. We see that, while s95p-PCE creates less radial flow, it generates a larger flow *anisotropy* (we checked this by direct computation), resulting in larger $v_2(p_T)$ for *both* pions and protons than with the other two equations of state. For EOS Q it was found in Refs. [15,16,19] that if the kinetic freeze-out temperature $T_{\rm dec}$ is adjusted to reproduce the p_T spectra, the correct implementation of chemical freeze-out at $T_{\rm chem}$ in the HRG phase increases the mass splitting between $v_2(p_T)$ of pions and protons at low p_T. On the other hand, if the freeze-out temperature is kept constant, the mass splitting at low p_T decreases [15]. Since we have kept the freeze-out temperature fixed in our calculations, we see a similar phenomenon here: The elliptic flow mass splitting between pions and protons is weaker for the chemically frozen s95p-PCE than for the chemically equilibrated EOS L and SM-EOS Q. This is a consequence of the weaker radial flow generated by s95p-PCE.

E. Dependence on the shape of the initial energy density profile (CGC vs. Glauber)

We close with a discussion of the influence of the shape of the initial energy density profile on the hadron spectra and elliptic flow, using the Glauber and CGC-fKLN models

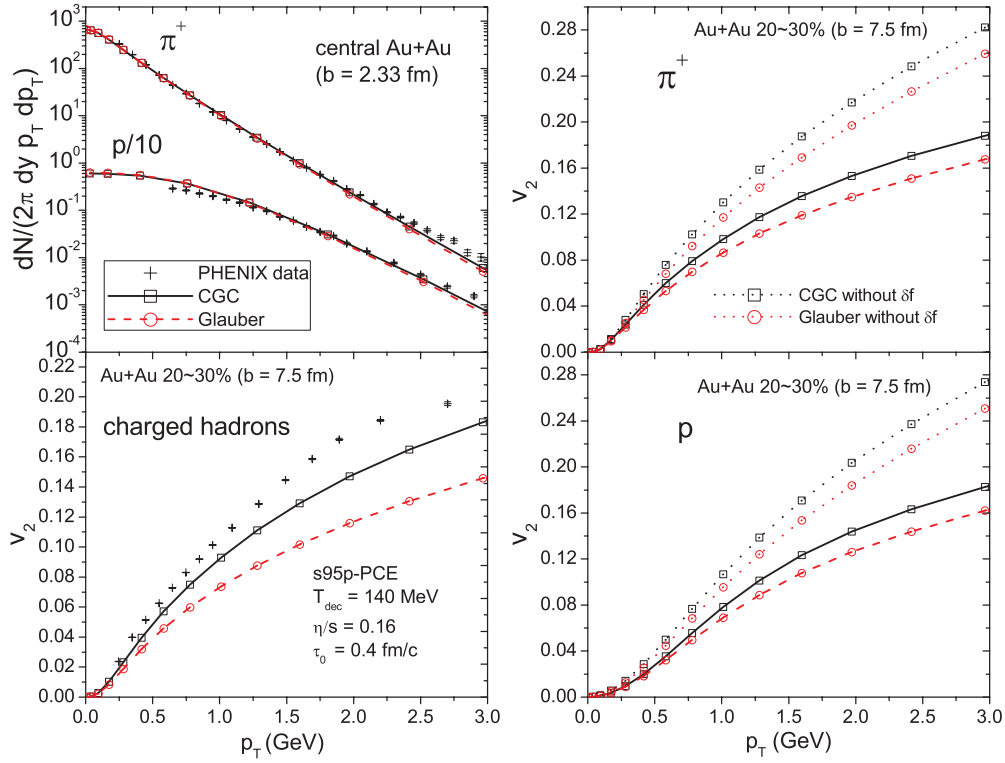

FIG. 8. (Color online) Similar to Fig. 4 but for fixed $\eta/s = 0.16$ and different initial energy density profiles (Glauber vs. CGC) as indicated. The elliptic flow from an initial CGC density profile is larger than for the Glauber initialization, due its larger initial eccentricity.

as examples. For an illustration of these profiles see Fig. 1.

The CGC profile is characterized by slightly steeper normalized energy density gradients than the Glauber profile. According to the Euler equation for ideal fluids

$$\dot{u}_\nu = \frac{c_s^2}{1+c_s^2}\frac{\nabla_\nu e}{e} \tag{7}$$

this leads to larger radial acceleration. Indeed, the upper left panel of Fig. 8 exhibits slightly flatter pion and proton spectra for CGC-initialized simulations than for Glauber initial conditions.

The elliptic flow coefficients for charged hadrons, pions, and protons are all significantly larger for the CGC-initialized runs than for Glauber initial conditions. This is a direct consequence of the well-known larger eccentricity of the CGC density profiles [10,50,58,60] which drives a larger momentum anisotropy. The effect is qualitatively similar for all hadron species. The small amount of added radial flow from the CGC initialization that we see in the spectra has very little influence on the p_T dependence of the proton v_2 when compared to the much larger effects coming from the larger source eccentricity. The suppression of v_2 by viscous δf corrections at freeze-out is similar for CGC and Glauber initial conditions, being slightly larger in the CGC case. This is presumably caused by the slightly larger flow velocities (and flow velicity gradients) generated by the CGC profile.

V. CONCLUSIONS

We have performed a systematic study of the dependence of the pion and proton transverse momentum spectra and their p_T-dependent elliptic flow on the thermalization time τ_0, initial energy density profile, equation of state, freeze-out temperature, and specific shear viscosity in $(2+1)$-dimensional viscous hydrodynamic simulations. Assuming a temperature-independent shear viscosity to entropy ratio and CGC initial conditions for the energy density profile, we find that the proton p_T spectra measured in 200A GeV central Au + Au collisions at RHIC favor η/s values between 2 and 3 times the KSS bound $(\frac{\eta}{s})_{\rm KSS} = \frac{1}{4\pi}$ while the p_T slope of the charged hadron elliptic flow prefers smaller values between 1 and 2 times the KSS bound. This tension cannot be resolved by different choices for the other paramaters whose variation we studied. Of course, the η/s values extracted from a comparison with simulations using the less eccentric Glauber model for the initial energy density profile are smaller, but the comparison with the experimental data gets worse (the proton spectra come out steeper) and tension between the η/s values preferred by spectra and v_2 gets stronger. Lower freeze-out temperatures improve the agreement with the data, in particular with the heavy-particle (proton) spectra. We saw very little sensitivity to the choice of the termalization time τ_0, but for larger values of τ_0 we did not allow for the evolution of pre-equilibrium radial and elliptic flow, contrary to what is expected to happen in reality. The main reason for not doing so was that, at this point, we have no theoretical

control over this pre-equilibrium flow, and we did not want to clutter our study by introducing still further parameters. If there is a tendency worth mentioning in the context of varying τ_0 it is that smaller τ_0 values lead to somewhat larger radial flow which helps with the description of heavy hadron spectra. This may, however, also be achievable by starting hydrodynamics later, but with nonzero initial transverse flow [21,84,85].

The main objective of this study was to gain an intuitive understanding what reasonable changes in the key parameters of a viscous hydrodynamic simulation will do to the final hadron spectra and elliptic flow. By also keeping an eye on the available experimental data we come to the conclusion that a purely hydrodynamic description of the experimental spectra will probably not work, at least not with temperature-independent η/s. Realistic variations of η/s with temperature are the subject of a separate study [36]. Based on that study combined with the one presented here we believe that giving up on a (viscous) hydrodynamic description of the hadron resonance gas stage and replacing it with a more reliable microscopic approach is unavoidable for a quantitative description of the experimental data.

ACKNOWLEDGMENTS

This work was supported by the US Department of Energy under contracts DE-SC0004286 and DE-AC02-05CH11231 and within the framework of the JET Collaboration under Grant No. DE-SC0004104. P.H.'s research was supported by the ExtreMe Matter Institute (EMMI). We thank Thomas Riley for helping us with the analytic parametrization of the EOS tables for s95p-PCE.

APPENDIX: ANALYTIC PARAMETRIZATION OF EOS s95p-PCE [68]

We used the following analytic parametrization for the equation of state s95p-PCE (energy density e and pressure p in GeV/fm^3, entropy density s in fm^{-3}, temperature T in GeV):

1. Pressure

$$p(e) = \begin{cases} 0.3299[\exp(0.4346e) - 1] & : \quad e < e_1 \\ 1.024 \times 10^{-7} \exp(6.041e) + 0.007273 + 0.14578e & : \quad e_1 < e < e_2 \\ 0.30195 \exp(0.31308e) - 0.256232 & : \quad e_2 < e < e_3 \\ 0.332e - 0.3223e^{0.4585} - 0.003906e \exp(-0.05697e) + 0.1167e^{-1.233} + 0.1436e \exp(-0.9131e) & : \quad e_3 < e < e_4 \\ 0.3327e - 0.3223e^{0.4585} - 0.003906e \exp(-0.05697e) & : \quad e > e_4 \end{cases} \tag{A1}$$

where $e_1 = 0.5028563305441270$ GeV/fm^3, $e_2 = 1.62$ GeV/fm^3, $e_3 = 1.86$ GeV/fm^3, and $e_4 = 9.9878355786273545$ GeV/fm^3.

2. Entropy density

$$s^{\frac{4}{3}}(e) = \begin{cases} 12.2304e^{1.16849} & : \quad e < e_1 \\ 11.9279e^{1.15635} & : \quad e_1 < e < e_2 \\ 0.0580578 + 11.833e^{1.16187} & : \quad e_2 < e < e_3 \\ \left.\begin{array}{l} 18.202e - 62.021814 - 4.85479 \exp(-2.72407 \times 10^{-11} e^{4.54886}) \\ +65.1272e^{-0.128012} \exp(-0.00369624e^{1.18735}) - 4.75253e^{-1.18423} \end{array}\right\} & : \quad e_3 < e < e_4 \\ \left.\begin{array}{l} 18.202e - 63.0218 - 4.85479 \exp(-2.72407 \times 10^{-11} e^{4.54886}) \\ +65.1272e^{-0.128012} \exp(-0.00369624e^{1.18735}) \end{array}\right\} & : \quad e > e_4 \end{cases} \tag{A2}$$

where $e_1 = 0.1270769021427449$ GeV/fm^3, $e_2 = 0.4467079524674040$ GeV/fm^3, $e_3 = 1.9402832534193788$ GeV/fm^3, and $e_4 = 3.7292474570977285$ GeV/fm^3.

3. Temperature

$$T(e) = \begin{cases} 0.203054e^{0.30679} & : \quad e < 0.5143939846236409 \text{ GeV/fm}^3 \\ (e + p)/s & : \quad e > 0.5143939846236409 \text{ GeV/fm}^3 \end{cases} \tag{A3}$$

[1] BRAHMS, I. Arsene *et al.*, Nucl. Phys. A **757**, 1 (2005).
[2] B. B. Back *et al.*, Nucl. Phys. A **757**, 28 (2005).
[3] J. Adams *et al.* (STAR Collaboration), Nucl. Phys. A **757**, 102 (2005).
[4] K. Adcox *et al.* (PHENIX Collaboration), Nucl. Phys. A **757**, 184 (2005).
[5] U. Heinz and P. F. Kolb, Nucl. Phys. A **702**, 269 (2002).
[6] P. F. Kolb and U. Heinz, Hydrodynamic description of ultrarelativistic heavy-ion collisions, in *Quark-Gluon Plasma 3*, edited by R. Hwa and X.-N. Wang (World Scientific, Singapore, 2004), p. 634.
[7] M. Gyulassy and L. McLerran, Nucl. Phys. A **750**, 30 (2005).
[8] P. Romatschke, Int. J. Mod. Phys. E **19**, 1 (2010).
[9] U. Heinz, Early collective expansion: Relativistic hydrodynamics and the transport properties of QCD matter, in *Relativistic Heavy Ion Physics*, edited by R. Stock, Landolt-Börnstein (Springer-Verlag, New York, 2010), Vol. I 23, chap. 5-1, arXiv:0901.4355 [nucl-th].
[10] M. Luzum and P. Romatschke, Phys. Rev. C **78**, 034915 (2008); **79**, 039903(E) (2009).
[11] R. A. Lacey *et al.*, Phys. Rev. C **82**, 034910 (2010).
[12] H. Song and U. Heinz, J. Phys. G: Part. Nucl. Phys. **36**, 064033 (2009).
[13] H. Song, Ph.D. thesis, The Ohio State University, 2009, arXiv:0908.3656 [nucl-th].
[14] F. Cooper and G. Frye, Phys. Rev. D **10**, 186 (1974).
[15] T. Hirano and K. Tsuda, Phys. Rev. C **66**, 054905 (2002).
[16] P. F. Kolb and R. Rapp, Phys. Rev. C **67**, 044903 (2003).
[17] P. Huovinen, Nucl. Phys. A **761**, 296 (2005).
[18] P. Huovinen and P. V. Ruuskanen, Annu. Rev. Nucl. Part. Sci. **56**, 163 (2006).
[19] P. Huovinen, Eur. Phys. J. A **37**, 121 (2008).
[20] K. J. Eskola, H. Niemi, and P. V. Ruuskanen, Phys. Rev. C **77**, 044907 (2008).
[21] W. Broniowski, M. Chojnacki, W. Florkowski, and A. Kisiel, Phys. Rev. Lett. **101**, 022301 (2008).
[22] P. Bozek and I. Wyskiel, Phys. Rev. C **79**, 044916 (2009).
[23] M. Cheng *et al.*, Phys. Rev. D **77**, 014511 (2008).
[24] A. Bazavov *et al.*, Phys. Rev. D **80**, 014504 (2009).
[25] P. Huovinen and P. Petreczky, Nucl. Phys. A **837**, 26 (2010).
[26] H. Bebie, P. Gerber, J. L. Goity, and H. Leutwyler, Nucl. Phys. B **378**, 95 (1992).
[27] D. Teaney, arXiv:nucl-th/0204023.
[28] P. Braun-Munzinger, D. Magestro, K. Redlich, and J. Stachel, Phys. Lett. B **518**, 41 (2001).
[29] A. Andronic, P. Braun-Munzinger, and J. Stachel, Phys. Lett. B **673**, 142 (2009); **678**, 516 (2009).
[30] R. A. Lacey and A. Taranenko, PoS **CFRNC2006**, 021 (2006).
[31] G. Policastro, D. T. Son, and A. O. Starinets, Phys. Rev. Lett. **87**, 081601 (2001).
[32] P. K. Kovtun, D. T. Son, and A. O. Starinets, Phys. Rev. Lett. **94**, 111601 (2005).
[33] L. P. Csernai, J. I. Kapusta, and L. D. McLerran, Phys. Rev. Lett. **97**, 152303 (2006).
[34] N. Demir and S. A. Bass, Phys. Rev. Lett. **102**, 172302 (2009).
[35] P. Bozek, Phys. Rev. C **81**, 034909 (2010).
[36] C. Shen *et al.* (to be published).
[37] H. Song and U. Heinz, Phys. Rev. C **78**, 024902 (2008).
[38] H. Song and U. Heinz, Phys. Rev. C **81**, 024905 (2010).
[39] U. Heinz, H. Song, and A. K. Chaudhuri, Phys. Rev. C **73**, 034904 (2006).
[40] W. Israel and J. M. Stewart, Ann. Phys. **118**, 341 (1979).
[41] A. Muronga, Phys. Rev. Lett. **88**, 062302 (2002).
[42] A. Muronga, Phys. Rev. C **69**, 034903 (2004).
[43] H. Song and U. Heinz, Phys. Lett. B **658**, 279 (2008).
[44] H. Song and U. Heinz, Phys. Rev. C **77**, 064901 (2008).
[45] P. F. Kolb, J. Sollfrank, and U. Heinz, Phys. Lett. B **459**, 667 (1999).
[46] P. F. Kolb, J. Sollfrank, and U. Heinz, Phys. Rev. C **62**, 054909 (2000).
[47] P. F. Kolb, U. Heinz, P. Huovinen, K. J. Eskola, and K. Tuominen, Nucl. Phys. A **696**, 197 (2001).
[48] D. Kharzeev and M. Nardi, Phys. Lett. B **507**, 121 (2001).
[49] D. Kharzeev, E. Levin, and M. Nardi, Nucl. Phys. A **730**, 448 (2004).
[50] A. Adil, H.-J. Drescher, A. Dumitru, A. Hayashigaki, and Y. Nara, Phys. Rev. C **74**, 044905 (2006).
[51] H. J. Drescher and Y. Nara, Phys. Rev. C **75**, 034905 (2007).
[52] R. P. G. Andrade, F. Grassi, Y. Hama, T. Kodama, and W. L. Qian, Phys. Rev. Lett. **101**, 112301 (2008).
[53] T. Hirano and Y. Nara, Phys. Rev. C **79**, 064904 (2009).
[54] H. Petersen and M. Bleicher, Phys. Rev. C **81**, 044906 (2010).
[55] H. Holopainen, H. Niemi, and K. J. Eskola, arXiv:1007.0368.
[56] B. Schenke, S. Jeon, and C. Gale, arXiv:1009.3244.
[57] H. Petersen, G.-Y. Qin, S. A. Bass, and B. Muller, arXiv:1008.0625.
[58] T. Hirano, U. Heinz, D. Kharzeev, R. Lacey, and Y. Nara, Phys. Lett. B **636**, 299 (2006).
[59] H.-J. Drescher, fKLN code, available at [http://th.physik.uni-frankfurt.de/∼drescher/CGC/].
[60] U. Heinz, J. S. Moreland, and H. Song, Phys. Rev. C **80**, 061901 (2009).
[61] J. Sollfrank, P. Koch, and U. Heinz, Phys. Lett. B **252**, 256 (1990).
[62] J. Sollfrank, P. Koch, and U. Heinz, Z. Phys. C **52**, 593 (1991).
[63] D. Teaney, Phys. Rev. C **68**, 034913 (2003).
[64] R. Baier, P. Romatschke, and U. A. Wiedemann, Phys. Rev. C **73**, 064903 (2006).
[65] K. Dusling, G. D. Moore, and D. Teaney, Phys. Rev. C **81**, 034907 (2010).
[66] Y. Aoki, Z. Fodor, S. D. Katz, and K. K. Szabo, J. High Energy Phys. 01 (2006) 089.
[67] M. Chojnacki and W. Florkowski, Acta Phys. Pol. B **38**, 3249 (2007).
[68] The EOS tables (by P. Huovinen), their analytic parametrizations (by T. Riley and C. Shen) and the list of included hadrons are available at the URLs [https://wiki.bnl.gov/hhic/index.php/Lattice_calculatons_of_Equation_of_State] and [https://wiki.bnl.gov/TECHQM/index.php/QCD_Equation_of_State].
[69] Particle Data Group, S. Eidelman *et al.*, Phys. Lett. B **592**, 1 (2004).
[70] C. M. Hung and E. V. Shuryak, Phys. Rev. Lett. **75**, 4003 (1995).
[71] D. Zschiesche, H. Stöcker, W. Greiner, and S. Schramm, Phys. Rev. C **65**, 064902 (2002).
[72] S. S. Adler *et al.* (PHENIX Collaboration), Phys. Rev. C **69**, 034909 (2004).
[73] S. Afanasiev *et al.* (PHENIX Collaboraton), Phys. Rev. C **80**, 024909 (2009).
[74] A. Adare *et al.* (PHENIX Collaboraton), Phys. Rev. Lett. **105**, 062301 (2010).
[75] U. Heinz, AIP Conf. Proc. **739**, 163 (2005).

[76] D. A. Teaney, J. Phys. G **30**, S1247 (2004).
[77] A. K. Chaudhuri and U. Heinz, J. Phys. Conf. Ser. **50**, 251 (2006).
[78] K. Dusling and D. Teaney, Phys. Rev. C **77**, 034905 (2008).
[79] P. Romatschke and U. Romatschke, Phys. Rev. Lett. **99**, 172301 (2007).
[80] E. Schnedermann, J. Sollfrank, and U. Heinz, NATO Adv. Study Inst. Ser. B Phys. **303**, 175 (1993).
[81] E. Schnedermann, J. Sollfrank, and U. Heinz, Phys. Rev. C **48**, 2462 (1993).
[82] T. Hirano and M. Gyulassy, Nucl. Phys. A **769**, 71 (2006).
[83] D. Teaney, J. Lauret, and E. V. Shuryak, arXiv:nucl-th/0110037.
[84] J. Vredevoogd and S. Pratt, Phys. Rev. C **79**, 044915 (2009).
[85] S. Pratt, Phys. Rev. Lett. **102**, 232301 (2009).